ACES Asian Chemical Editorial Society

DOI: 10.1002/cnma.201600359

CHEMNANOMAT
Full Paper

Noble Metal Nanocrystals

Bifunctional $Ag@SiO_2$/Au Nanoparticles for Probing Sequential Catalytic Reactions by Surface-Enhanced Raman Spectroscopy

Yiren Wu,[a] Dong Su,[b] and Dong Qin*[a]

Abstract: We report the synthesis of bifunctional $Ag@SiO_2$/Au nanoparticles with an "islands in the sea" configuration by titrating $HAuCl_4$ solution into an aqueous suspension of $Ag@SiO_2$ core–shell nanocubes in the presence of NaOH, ascorbic acid, and poly(vinyl pyrrolidone) at pH 11.9. The NaOH plays an essential role in generating small pores in the SiO_2 shell *in situ*, followed by the epitaxial deposition of Au from the Ag surface through the pores, leading to the formation of Au islands (6–12 nm in size) immersed in a SiO_2 sea. By controlling the amount of $HAuCl_4$ titrated into the reaction system, the Au islands can be made to pass through and protrude from the SiO_2 shell, embracing catalytic activity toward the reduction of 4-nitrophenol to 4-aminophenol by $NaBH_4$. While the Ag in the core provides a strong surface-enhanced Raman scattering activity, the SiO_2 sea helps maintain the Au component as compact, isolated, and stabilized islands. The $Ag@SiO_2$/Au nanoparticles can serve as a bifunctional probe to monitor the stepwise Au-catalyzed reduction of 4-nitrothiophenol to 4-aminothiophenol by $NaBH_4$ and Ag-catalyzed oxidation of 4-aminothiophenol to *trans*-4,4′-dimercaptoazobenzene by the O_2 from air in the same reaction system.

Introduction

Noble-metal nanocrystals have found applications in areas ranging from catalysis to photonics, electronics, sensing, imaging, and biomedical research.[1–5] Bimetallic nanocrystals, in particular, have received ever growing interest in recent years because of their enhanced properties relative to their monometallic counterparts.[6–10] By controlling the ratio and spatial distributions of the elements, one can engineer and enrich the properties of bimetallic nanocrystals to greatly expand their scope of applications. One intriguing bimetallic system is based upon Ag and Au. Silver nanocrystals exhibit localized surface plasmon resonance (LSPR) in the visible region for surface-enhanced Raman scattering (SERS),[11,12] and they can also serve as a superb catalyst for oxidation reactions, including the epoxidation of ethylene by O_2.[13] On the other hand, Au is well-known for its intrinsic inertness. However, it has been demonstrated that the catalytic activity of Au can be drastically enhanced by substantially downsizing the nanoparticles.[14–17] To this end, Haruta and co-workers discovered that the catalytic activity of TiO_2-supported Au nanoparticles toward CO oxidation increased significantly as their sizes were reduced down to 5 nm and below.[15] In principle, by simply coating the surface of Ag nanocrystals with discrete Au islands of less than 5 nm in size, one could design a useful bimetallic system with a unique integration of SERS and catalytic properties originating from the Ag and Au components, respectively.

Although it appears straightforward to prepare the aforementioned Ag–Au bimetallic system, the synthesis inherits a number of challenges. For of all, the galvanic replacement between Ag and $AuCl_4^-$ precludes the use of a protocol that involves the reduction of $AuCl_4^-$ in the presence of Ag nanocrystals.[18] Even when the galvanic replacement is suppressed through the introduction of a strong reducing agent, the deposition of Au atoms tends to take a layer-by-layer rather than island growth mode.[19] It is possible to deposit pre-synthesized Au nanoparticles onto the surface of Ag nanocrystals through careful manipulation of surface charges, but it will be difficult to prevent the Au nanoparticles from touching and merging into larger structures. In addition, the tiny Au particles with an enormous surface-to-volume ratio have a strong tendency to coagulate during operation, ultimately losing their catalytic activity. One approach to improving the stability against coagulation is to encapsulate the Au nanoparticles with a thin, porous oxide layer, such as SiO_2, SnO_2, CeO_2, or TiO_2. To this end, it has been demonstrated that the oxide layer could serve as a physical barrier to isolate and confine the metal nanoparticles for a variety of systems.[19–25] However, the presence of an oxide layer tends to block the active sites on metal nanoparticles, leading to reduction in catalytic activity when compared with the naked metal nanoparticles.

[a] *Y. Wu, Dr. D. Qin*
School of Materials Science and Engineering
Georgia Institute of Technology
Atlanta, Georgia 30332 (United States)
E-mail: dong.qin@mse.gatech.edu

[b] *Dr. D. Su*
Center for Functional Nanomaterials
Brookhaven National Laboratory
Upton, New York 11973 (United States)

Supporting information and the ORCID identification number(s) for the author(s) of this article can be found under http://dx.doi.org/10.1002/cnma.201600359.

Herein, we report a rational approach to the synthesis of $Ag@SiO_2/Au$ nanoparticles that consist of Au nanoparticles on the surface of Ag nanocubes that are isolated from each other, but not fully covered, by SiO_2. We start with a Stöber process to deposit a thin layer of SiO_2 on the surface of Ag nanocubes to generate $Ag@SiO_2$ core–shell nanocubes.[26] We then titrate aqueous $HAuCl_4$ into an aqueous suspension containing the $Ag@SiO_2$ nanocubes, ascorbic acid (AA, a reducing agent), poly(vinyl pyrrolidone) (PVP, a colloidal stabilizer), and NaOH at pH 11.9. The OH^- ions can chemically etch the SiO_2 shell to generate pathways for the reagents to directly access the surface of the Ag nanocube.[27] In the presence of AA, $AuCl_4^-$ could be reduced to generate $AuCl_2^-$.[28] The galvanic replacement reaction between Au^{3+}/Au^+ and Ag then quickly initiates the nucleation and deposition of Au atoms on the surface of Ag nanocube. Afterwards, the pores within the SiO_2 shell are gradually filled by the Au atoms derived from the reduction of Au^{3+}/Au^+ by AA, leading to the formation of discrete, well-defined Au islands immersed in a sea made of SiO_2. We confirm the catalytic activity of the Au islands using the reduction of 4-nitrophenol (4-NP) to 4-aminophenol (4-AP) by $NaBH_4$. We also demonstrate that the bimetallic nanoparticles exhibit SERS activity, which is 10-fold stronger than that of the $Ag@SiO_2$ nanocubes. Remarkably, the integrated catalytic and SERS properties of these nanoparticles can be used for *in situ* SERS probing of the Au-catalyzed reduction of 4-nitrothiophenol (4-NTP) by $NaBH_4$ and the Ag-catalyzed oxidation of 4-aminothiophenol (4-ATP) by O_2 from air.

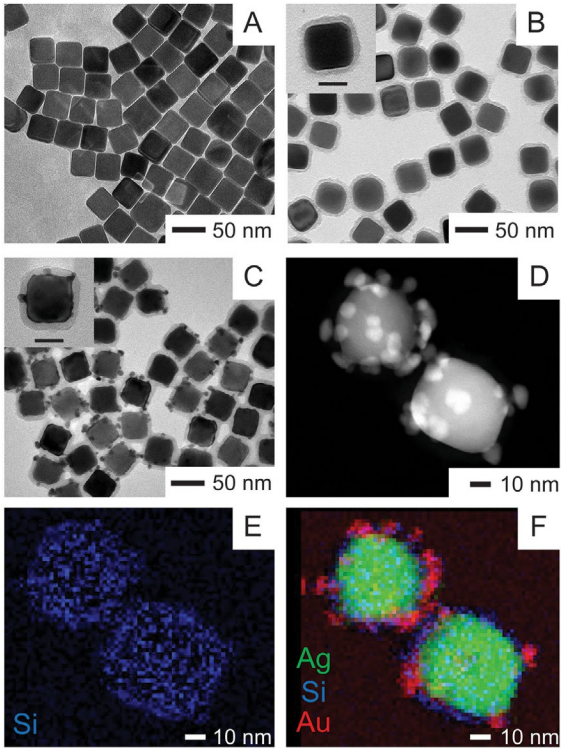

Figure 1. TEM images of (A) Ag nanocubes, (B) $Ag@SiO_2$ nanocubes, and (C) $Ag@SiO_2/Au$ nanoparticles prepared with the titration of 0.4 mL of 0.1 mM aqueous $HAuCl_4$. (D) HAADF-STEM image and (E,F) EELS mapping images of the $Ag@SiO_2/Au$ nanoparticles.

Results and Discussion

We followed the published protocols to synthesize the Ag nanocubes (Figure 1A) with an edge length of 38.6 ± 1.8 nm and the $Ag@SiO_2$ nanocubes (Figure 1B) with an oxide shell of 6.0 ± 0.2 nm in thickness, respectively.[29,30] We then dispersed the $Ag@SiO_2$ nanocubes in an aqueous solution containing AA, PVP, and NaOH at pH 11.9, followed by the titration of aqueous $HAuCl_4$ using a syringe pump at a relatively slow rate under ambient conditions. Figure 1C shows a TEM image of the sample obtained after the titration of 0.4 mL aqueous $HAuCl_4$, indicating the formation of Au islands, with sizes ranging from 6 to 12 nm in diameter, over the surface of each $Ag@SiO_2$ nanocube. It should be pointed out that the thickness of the SiO_2 shell remained essentially the same during the transformation of $Ag@SiO_2$ nanocubes into $Ag@SiO_2/Au$ nanoparticles (see the insets of Figure 1B and C). Figure 1D shows a high-angle annular dark field scanning TEM (HAADF-STEM) image of two $Ag@SiO_2/Au$ nanoparticles, from which we could simply distinguish Au from Ag by contrast. As shown in Figure 1E and F, electron energy-loss spectroscopy (EELS) mapping of these two nanoparticles clearly confirmed the generation of discrete Au islands directly on the surface of each Ag nanocube, with SiO_2 serving as a spacer among the islands.

We also used high-resolution HAADF-STEM to resolve the interface at which the growth of Au was instigated. As shown in Figure 2A and B, the Au atoms directly nucleated and grew from the surface of the Ag nanocube encapsulated in the SiO_2 shell. Figure 2C–E shows the STEM-EELS mapping of Au, Ag, and Si, respectively. We confirmed that the initial deposition of Au atoms was indeed initiated from the surface of the Ag nanocube, followed by the continuous growth into a Au island (Figure 2C). There was a detectable layer of Ag on top of the outermost surface of the Au island (Figure 2D). The silica layer was retained on the surface of the Ag nanocube, with very little coverage on the Au island (Figure 2E). However, it is diffi-

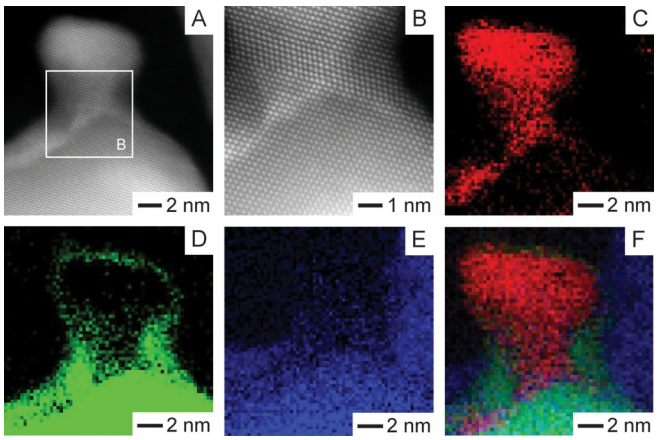

Figure 2. (A,B) HAADF-STEM images, at two different magnifications, of a Au island on the surface of a $Ag@SiO_2/Au$ nanoparticle that was prepared with the titration of 0.4 mL of 0.1 mM aqueous $HAuCl_4$. (C–F) STEM-EELS elemental mapping of Au (red), Ag (green), and Si (blue), respectively, of the Au island.

cult, if not impossible, to clearly resolve any silica layer on the outermost surface of the Au island. Taken together, we believe that the Au nanoparticles and SiO_2 shell were situated on the surface of each Ag nanocube with an "islands in a sea" configuration (Figure 2F).

Figure 3 illustrates a mechanism proposed to account for the formation of Ag@SiO_2/Au nanoparticles. In the first step, small pores are generated *in situ* in the SiO_2 shell due to chemical etching by NaOH.[27] We argue that such pores ultimately determine the sites for the nucleation and epitaxial growth of Au islands on the surface of each Ag nanocube. In the second step, upon the titration of aqueous $HAuCl_4$ in the presence of AA, it is possible that Au^{3+} would be reduced to generate Au^+.[28] These Au^{3+}/Au^+ ions would diffuse through the pores to react with the Ag surface via galvanic replacement for the initial deposition of Au atoms on the surface of each Ag nanocube at the expense of Ag atoms from the nanocube, leading to the formation of a Ag core slightly deviating from the cubic shape (see Figure 1C). We suspect that these dissolved Ag^+ ions could then react with OH^- for the generation of Ag_2O patches on the surface of Ag nanocubes, preventing the underlying Ag from further reaction with Au^{3+}/Au.[31] In the third step, as the titration of $HAuCl_4$ is continued, the Au atoms derived from the reduction of Au^{3+}/ Au^+ by both AA and Ag will result in the formation of Au islands that pass through and eventually protrude from the SiO_2 shell, leading to the generation of Ag@SiO_2/Au nanoparticles with an "islands in the sea" structure. Likely, some Ag^+ ions in the reaction solution were, in turn, reduced by AA to generate Ag atoms, followed by their deposition onto the surface of Au islands (see Figure 2D). These results also support our argument that the AA was in proximity to the surface of Ag nanocubes, facilitating the reduction of Au^{3+}/Au^+ ions for the continuous growth of Au islands as more $HAuCl_4$ was titrated into the reaction solution. It is worth mentioning that, during the growth of Au islands, the galvanic replacement reaction would create new sites for the epitaxial growth of more Au islands on the surface of each Ag nanocube. As a result, we obtained Ag@SiO_2/Au nanoparticles with variations in both number and size for the Au islands among different particles (see Figure 1C).

To further validate our hypothesis, we collected another two data points with the titration volume of $HAuCl_4$ at 0.2 and 0.8 mL while keeping all other experimental parameters unaltered. Figure S1 in the Supporting Information shows TEM and SEM images of the as-obtained samples. With an increase in titration volume, the products showed increase in both the coverage of Au islands on each Ag nanocube and the size of individual Au islands. Our inductively coupled plasma mass spectroscopy (ICP-MS) analyses indicate that 88% of the added $HAuCl_4$ was reduced to Au atoms, followed by their deposition onto the Ag nanocubes. As expected, the longer reaction time for the case of 0.8 mL of $HAuCl_4$ would create more nucleation sites for the growth of Au islands, in addition to their increase in size. We also used XPS to analyze the Au deposited on the Ag nanocubes (Figure S2). We found that the amount of Au increased with the titration volume. Additionally, the gaps between the $3d_{5/2}$ and $3d_{3/2}$ peaks of Ag ($\Delta = 6.0$ eV) and those between the $4f_{7/2}$ and $4f_{5/2}$ peaks of Au ($\Delta = 3.7$ eV) are exactly the same as the values for zero-valent Au and Ag (Table S1),[32] suggesting the presence of Au and Ag atoms in a zero-valent state for both samples. During the titration process, we found that the pH dropped slightly from 11.9 to 11.7, 11.3, 10.2 at titration of volumes of 0.2, 0.4, 0.8 mL, respectively. As a result, we believe that the reducing power of AA would drop slightly during the titration process. To further understand the role of pH in controlling the generation of Ag@SiO_2/Au nanoparticles, we performed another experiment by titrating aqueous $HAuCl_4$ into an aqueous suspension of Ag@SiO_2 in the presence of AA and PVP at pH 10.3, with the involvement of 300 μL NaOH (200 mM). Figure S3 shows a TEM image of the product obtained by at a titration volume of 0.8 mL of $HAuCl_4$, which is similar to those shown in Figure S1C. We also conducted a control experiment by titrating aqueous $HAuCl_4$ into an aqueous suspension of Ag@SiO_2 in the presence of AA and PVP only at pH 3.1, without the involvement of any NaOH. As shown in Figure S4, we observed a mixture of Ag@SiO_2 nanocubes and Au nanoparticles for 0.4 mL and 0.8 mL of $HAuCl_4$, respectively. In this case, the Au nanoparticles were formed through homogenous nucleation and growth upon the reduction by AA. Collectively, these results offer addition evidence to support the proposed mechanism.

We confirmed the catalytic activity of the Au islands using the reduction of 4-NP to 4-AP by $NaBH_4$.[33] We prepared two samples by fixing the number of Ag@SiO_2 nanocubes at $\approx 10^{11}$

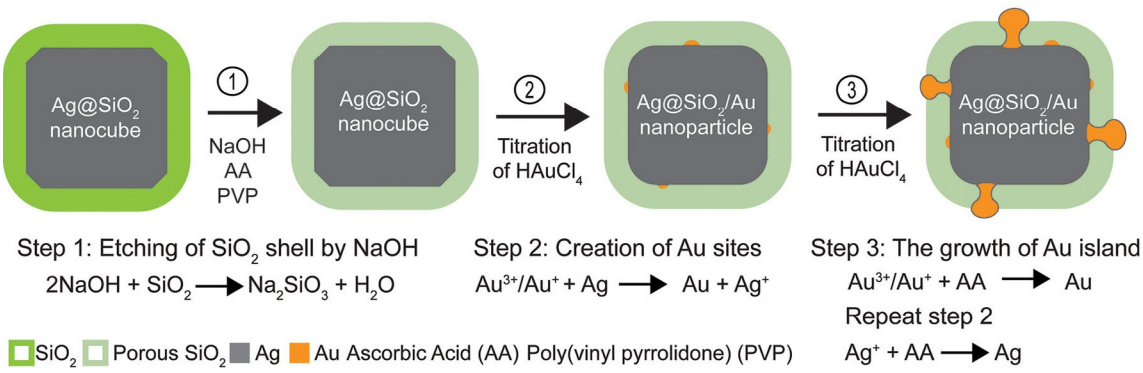

Figure 3. Schematic illustration of all the major steps and reactions involved in the fabrication of Ag@SiO_2/Au nanoparticles.

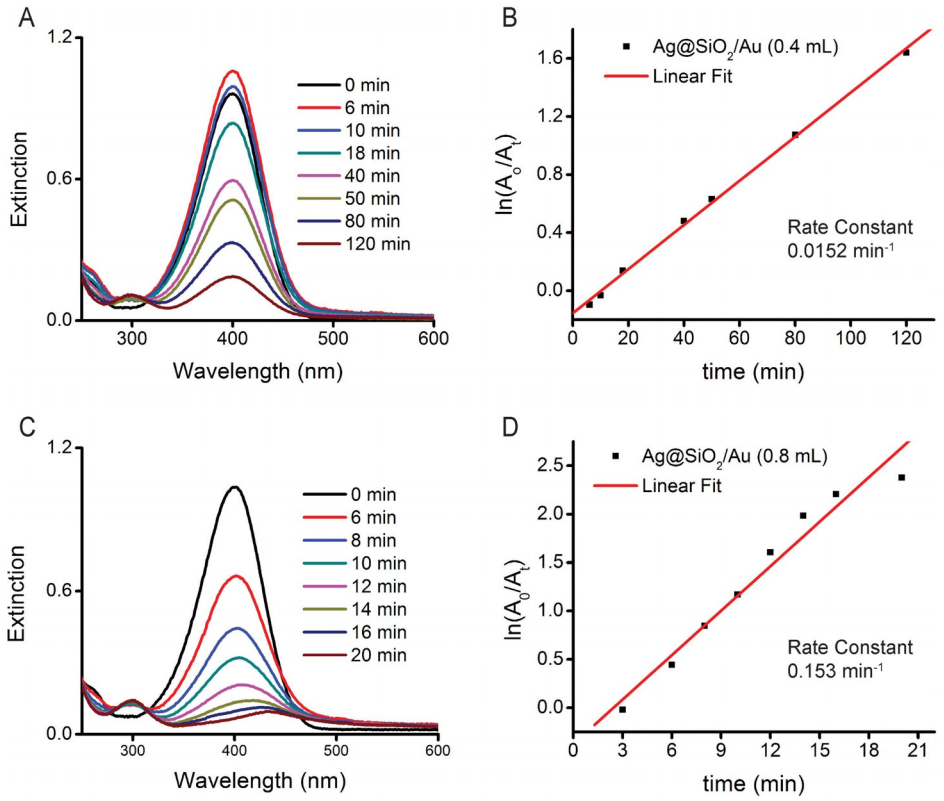

Figure 4. (A, C) UV-vis spectra recorded at different time intervals for the reduction of 4-NP by $NaBH_4$ at room temperature, in the presence of $Ag@SiO_2/Au$ nanoparticles as a catalyst. The catalysts were prepared with the titration of (A) 0.4 mL and (C) 0.8 mL of 0.1 mM $HAuCl_4$ solution. (B, D) Plots of $\ln[A_0/A_t]$ versus time for the peaks located at 400 nm in (A) and (C), respectively.

to obtain $Ag@SiO_2/Au$ nanoparticles at titration volumes of 0.4 mL and 0.8 mL, respectively. The as-obtained samples were directly added as catalysts. Upon the introduction of $NaBH_4$, we collected UV-vis spectra of 4-NP at different intervals of time (Figure 4A and C). By monitoring the absorption peak at 400 nm, we plotted $\ln(A_t/A_0)$ as a function of reaction time (Figure 4B and D). In both cases, the reduction reaction exhibited first-order kinetics, and as a result, we obtained the rate constant through curve fitting. For the $Ag@SiO_2/Au$ nanoparticles prepared at 0.4 mL and 0.8 mL of $HAuCl_4$, the rate constants were 0.015 min^{-1} and 0.15 min^{-1}, respectively. These results indicate that the reduction would be accelerated by 10 times when we doubled the titration volume of $HAuCl_4$. As demonstrated in Figure S5, the rate constant was further increased to 0.27 min^{-1} when we doubled the number of catalytic particles prepared at 0.8 mL of $HAuCl_4$. These data support our argument that a greater titration volume of the $AuCl_4^-$ precursor would increase both the number and size of Au islands on the surface of each Ag nanocube, ultimately accelerating the reduction kinetics of 4-NP.

For the $Ag@SiO_2/Au$ nanoparticles prepared with 0.8 mL of $HAuCl_4$, we also evaluated their catalytic stability for the reduction of 4-NP by $NaBH_4$. Specifically, after one round of reaction, we collected the catalytic particles and applied them to another round of reaction. As shown in Figure S6A, the rate constant dropped from 0.069 to 0.049, and 0.023 min^{-1} after one, two, and three rounds of reaction, respectively. We also collected UV-vis spectra from the $Ag@SiO_2/Au$ nanoparticles after each round of reaction by collecting the solids by centrifugation and re-dispersing them in the same amount of water. As shown in Figure S6B, the LSPR peak intensity dropped while the peak position remained unchanged. The drop in LSPR peak intensity can be attributed to the loss of nanoparticles during the centrifugation process. The structure and morphology of the nanoparticles should remain unchanged because the LSPR peak position changed very little. This data are consistent with what is shown in Figure S5. When the number of catalytic particles was doubled, the rate constant was almost doubled, increasing from 0.15 to 0.27 min^{-1}. In fact, when we normalized the rate constant against the number of catalytic particles (based on the LSPR peak intensities in Figure S6B), the rate constants became 0.11, and 0.073, and 0.034 for the first, second, and third rounds of reaction.

We also characterized the LSPR properties of the $Ag@SiO_2/Au$ nanoparticles. Figure 5 shows the UV-vis spectra recorded from aqueous suspensions of the Ag nanocubes, $Ag@SiO_2$ nanocubes, and the as-obtained $Ag@SiO_2/Au$ nanoparticles prepared at titration volumes of 0.4 mL and 0.8 mL, respectively, for $HAuCl_4$. For the Ag nanocubes, the UV-vis spectrum showed a strong peak at 440 nm (peak #1), one shoulder at 386 nm (peak #2), and a weak peak at 348 nm (peak #3). Calculations based on the discrete dipole approximation (DDA) method indicates that the physical origins of peaks #1 and #2 can be attributed to dipole resonances,[34] while peak #3 is par-

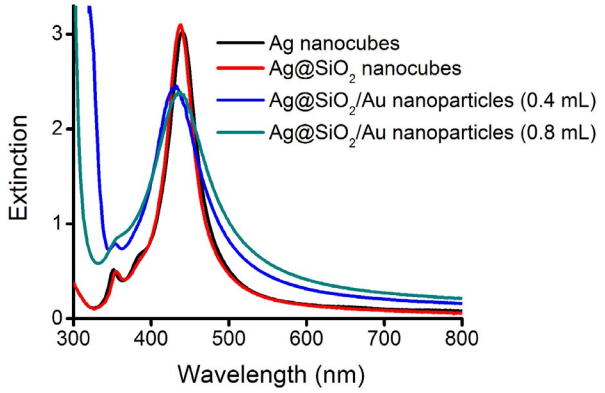

Figure 5. UV-vis spectra recorded from aqueous suspensions of Ag nanocubes, $Ag@SiO_2$ nanocubes, and $Ag@SiO_2$/Au nanoparticles prepared with the titration of 0.4 mL and 0.8 mL of 0.1 mM $HAuCl_4$ solution.

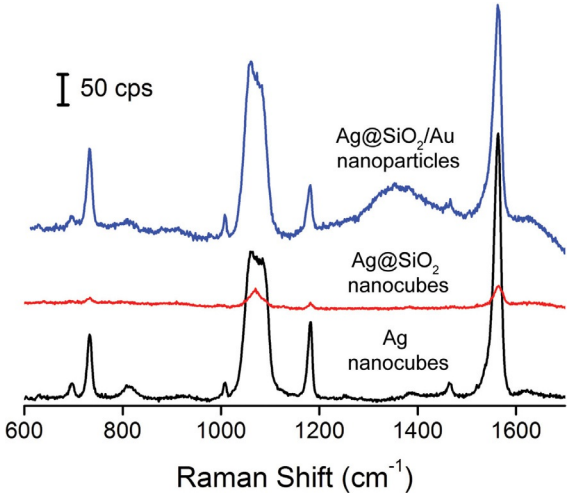

Figure 6. SERS spectra collected from 1,4-BDT immobilized on Ag nanocubes, $Ag@SiO_2$ nanocubes, and $Ag@SiO_2$/Au nanoparticles with an excitation wavelength at 532 nm. The $Ag@SiO_2$/Au nanoparticles were prepared with 0.4 mL of 0.1 mM $HAuCl_4$ solution.

ticularly sensitive to the sharpness of edges and corners of a Ag nanocube. The major dipole resonance (peak #1) was slightly blueshifted from 440 to 438 nm while peak #2 slightly dropped in intensity after SiO_2 coating due to the change in dielectric constant caused by the oxide layer and the slight truncation at the corner and edge sites (Figure 1B). After the titration of 0.4 mL of $HAuCl_4$, peak #1 was further shifted to 433 nm, together with a decrease in intensity for peak #3. Such changes in the LSPR spectrum can be attributed to the increase in truncation at the corner and edge sites (Figure 1D). When the volume of $HAuCl_4$ was increased to 0.8 mL, peak #1 was slightly redshifted from 433 to 438 nm, together with broadening in width. Both changes can be attributed to the increase in both number and volume for the Au islands on each Ag nanocube. Also, peak #3 became undetectable due to continuous truncation to the corners and edges of the Ag core. Collectively, the LSPR spectra also support our results of morphology characterization (see Figure 1).

We benchmarked the SERS activity of the $Ag@SiO_2$/Au nanoparticles against those of both Ag and $Ag@SiO_2$ nanocubes. In a typical measurement, we functionalized the nanoparticles with 1,4-benzenedithiol (1,4-BDT) and then collected SERS spectra from their suspensions at an excitation wavelength of 532 nm. As shown in Figure 6, the SERS activity of the Ag nanocubes dropped significantly after their surface had been coated with a SiO_2 shell of 6 nm thick. For instance, the intensity of the benzene ring mode at 1564 cm^{-1} decreased by 93.1%, primarily due to the blocking of Ag surface by SiO_2 shell toward the binding of 1,4-BDT probe molecules. Interestingly, some 1,4-BDT molecules could still be trapped in the SiO_2 shell and/or physically adsorbed on the surface, contributing to the observation of weak SERS signals, because these molecules could still feel the enhanced electromagnetic field on the Ag core.[35] Upon the growth of Au islands in the SiO_2 shells, the intensity of the peak at 1564 cm^{-1} was brought back to a level comparable to that of the Ag nanocubes, corresponding to a 10-fold enhancement relative to that of the $Ag@SiO_2$ nanocubes. In this case, the 1,4-BDT probe molecules were anticipated to bind to the surface of the Au islands. Since the Au islands were directly anchored on the surface of the Ag nanocube, hot spots could be formed at their tips to yield strong SERS.[36,37]

By leveraging the catalytic activity of the Au islands and the SERS activity of the Ag core, we further demonstrated the use of the $Ag@SiO_2$/Au nanoparticles for *in situ* SERS monitoring of the reduction of 4-NTP by $NaBH_4$. In a typical experiment, we prepared $Ag@SiO_2$/Au nanoparticles with 0.4 mL of $HAuCl_4$ and then functionalized their surfaces with 4-NTP (see Experimental Section for details). After initiating the reaction with $NaBH_4$, we collected SERS spectra from the reaction solution at different time intervals at an excitation of 532 nm (Figure 7). At $t=0$, the SERS spectrum shows three characteristic bands of 4-NTP at 1109 cm^{-1} (C–N stretching, ν_{CN}), 1338 cm^{-1} (O–N–O stretching, ν_{NO2}), and 1572 cm^{-1} (C–C stretching, ν_{CC}). The peak located at 1082 cm^{-1} can be assigned to the C–S stretching, ν_{CS}. At $t=9$ min, we observed the shift of ν_{NO2} peak from 1338 cm^{-1} to 1328 cm^{-1}, together with a significant drop in peak intensity. For instance, the intensity of ν_{NO2} at 1338 cm^{-1} or ν_{CC} at 1572 cm^{-1} decreased by 94% or 93%, respectively. We suspected that some of the 4-NTP adsorbed on Au islands could be released by $NaBH_4$ due to a stronger binding of BH_4^- to Au surface.[38] At $t=22$ min, the three characteristic bands of 4-NTP could no longer be resolved from the spectrum. On the other hand, we observed a small peak at 1594 cm^{-1}, which can be assigned to the ν_{CC} of 4-ATP. Based on our previous findings, the intensity of ν_{CC} for 4-ATP could become one order of magnitude weaker than that of the band for 4-NTP after the reduction of 4-NTP to 4-ATP by $NaBH_4$.[39–41] From the presence of ν_{CS} band at 1082 cm^{-1}, we argued that some of the 4-ATP molecules were adsorbed on the Au surface. From 22 to 66 min, the SERS spectra remained essentially unaltered. At $t=$ 89 min, four peaks emerged at 1142, 1387, 1429, and 1574 cm^{-1}, which could be assigned to the $\nu_{CN}+\beta_{CH}$, $\nu_{NN}+\nu_{CN}$, $\nu_{NN}+\beta_{CH}$, and ν_{CC} of *trans*-4,4′-dimercaptoazobenzene (*trans*-DMAB), respectively. This result suggests the oxidation of 4-ATP to *trans*-DMAB by the O_2 from air. At $t=120$ min, the spec-

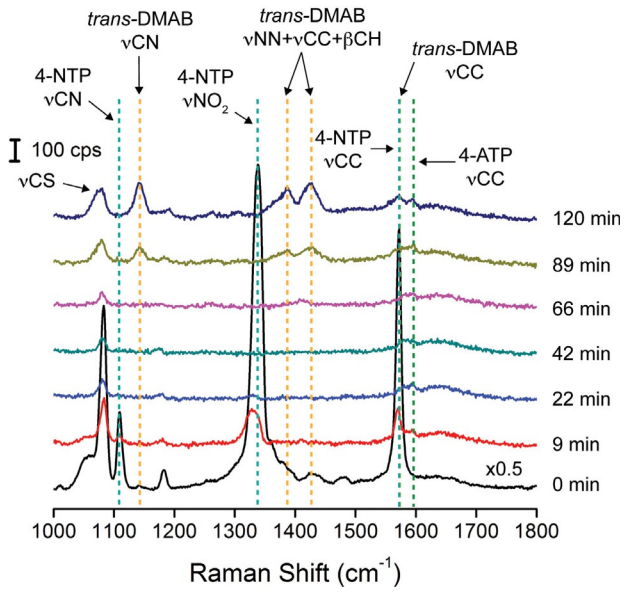

Figure 7. SERS spectra collected before and after the introduction of $NaBH_4$ solution into an aqueous suspension of 4-NTP-functionalized $Ag@SiO_2/Au$ nanoparticles at an excitation wavelength of 532 nm. The nanoparticles were prepared with the titration of 0.4 mL of 0.1 mM $HAuCl_4$ solution.

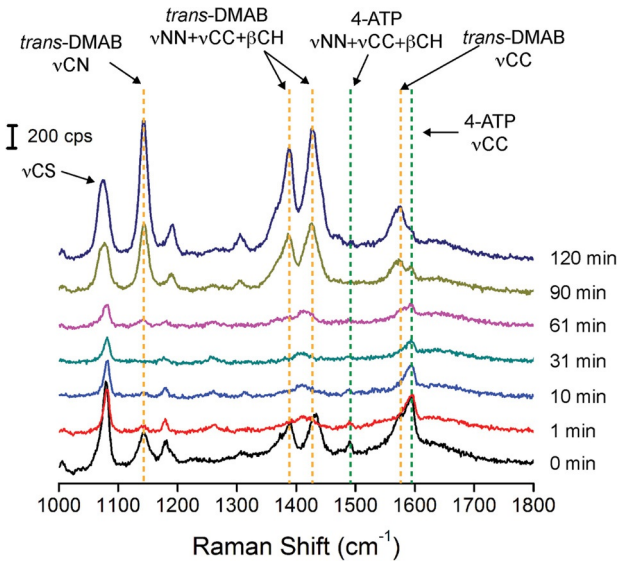

Figure 8. SERS spectra recorded before and after the introduction of $NaBH_4$ solution into an aqueous suspension of $Ag@SiO_2/Au$ nanoparticles functionalized with 4-ATP as a SERS probe molecule. The nanoparticles were prepared with the titration of 0.4 mL of 0.1 mM $HAuCl_4$ solution.

trum remained essentially the same except for a slight increase in intensity for the peaks. Taken together, we believe that the Au islands could serve as a catalyst to facilitate the reduction of 4-NTP by $NaBH_4$.[39] Once $NaBH_4$ was completely consumed in the reaction solution, the Ag atoms in the outmost surface could activate O_2 in the aqueous solution for the oxidation of 4-ATP to *trans*-DMAB.[41]

To gain a better mechanistic insight into the oxidation of 4-ATP to *trans*-DMAB on the surface of the $Ag@SiO_2/Au$ nanoparticles, we directly functionalized the surface of the nanoparticles (obtained at a titration volume of 0.4 mL) with 4-ATP and then recorded the SERS spectra. As shown in Figure S7 we also observed the four peaks of *trans*-DMAB at 1142 cm^{-1}, 1390 cm^{-1}, 1430 cm^{-1}, and 1576 cm^{-1}, together with two peaks of 4-ATP peaks at 1595 and 1489 cm^{-1}, suggesting that some of the immobilized 4-ATP could be oxidized by the O_2 from air to generate *trans*-DMAB. This observation is consistent with previous findings.[42,43] When the solution was left in the air for up to 120 min, the intensities of peaks from *trans*-DMAB were found to continuously increase with no change to the peak positions. Interestingly, we can reduce the *trans*-DMAB back to 4-ATP by adding $NaBH_4$. As shown in Figure 8, upon the introduction of $NaBH_4$, the four characteristic peaks of *trans*-DMAB (marked in yellow) disappeared after 1 min. The remaining two peaks can be assigned to 4-ATP (marked in green). From 1 to 60 min, the SERS spectra showed very minor changes except that the two peaks of 4-ATP dropped in intensity, likely due to the desorption of 4-ATP caused by $NaBH_4$ as we discussed previously.[38] At $t = 90$ min, the peaks of *trans*-DMAB returned. At this point, all the $NaBH_4$ had been consumed and 4-ATP was oxidized back to *trans*-DMAB by the O_2 from air. At $t = 120$ min, the peak positions remained the same but the intensities of all bands dropped, consistent with our previous observation (see Figure 7).

Conclusions

In summary, we have demonstrated a rational approach to the synthesis of $Ag@SiO_2/Au$ nanoparticles through the titration of $HAuCl_4$ into an aqueous suspension of $Ag@SiO_2$ core–shell nanocubes in the presence of AA, PVP, and NaOH at pH 11.9. Both HAADF-STEM and EELS studies confirm the growth of Au islands (with sizes in the range of 6 to 12 nm) directly from the surface of each Ag nanocube, passing through the SiO_2 shell to generate an "islands in the sea" structure. In this synthesis, NaOH plays a critical role in creating some initial pores in the SiO_2 shell on each Ag nanocube. The salt precursor reacts with Ag through galvanic replacement to initiate the nucleation of Au, followed by continuous reduction by AA and Ag for epitaxial growth into discrete Au islands that eventually pass through and protrude from the SiO_2 shell. The SiO_2 surrounding the Au islands helps confine them to a small size while preventing them from coalescing into larger structures. The Au islands show strong catalytic activity toward the reduction of 4-NP by $NaBH_4$. Because the Au islands are directly attached to the surface of the Ag nanocube, the $Ag@SiO_2/Au$ nanoparticles also exhibit strong SERS activity comparable to that of the pristine Ag nanocubes. By integrating the catalytic and SERS activities originating from the Au islands and Ag cores, respectively, we demonstrated the fabrication of a bifunctional probe for *in situ* monitoring the Au-catalyzed reduction of 4-NTP by $NaBH_4$ and subsequently the Ag-catalyzed oxidation of 4-ATP by the O_2 from air. The strategy demonstrated in this work can be potentially extended to other noble metals other than Au to further expand the range of catalytic reactions.

Acknowledgements

We acknowledge the support from the National Science Foundation (CHE-1412006), start-up funds from the Georgia Institute of Technology (GT), and a 3M non-tenured faculty award. We thank J. Ahn and K. D. Gilroy for performing the ICP-MS and XPS analyses. We acknowledge the use of electron microscopy resources at the Center for Functional Nanomaterials, a U.S. DOE Office of Science Facility, at Brookhaven National Laboratory under Contract No. DE-SC0012704.

Keywords: Ag@SiO_2 nanocrystals · silver-catalyzed oxidation · gold-catalyzed reduction · gold nanoparticles · surface-enhanced Raman scattering

[1] M. A. El-Sayed, *Acc. Chem. Res.* **2001**, *34*, 257 – 264.
[2] M. R. Jones, K. D. Osberg, R. J. Macfarlane, M. R. Langille, C. A. Mirkin, *Chem. Rev.* **2011**, *111*, 3736 – 3827.
[3] A. J. Haes, C. L. Haynes, A. D. McFarland, G. C. Schatz, R. P. Van Duyne, S. Zou, *MRS Bull.* **2005**, *30*, 368 – 375.
[4] S. Lal, S. E. Clare, N. J. Halas, *Acc. Chem. Res.* **2008**, *41*, 1842 – 1851.
[5] Y. Xia, W. Li, C. M. Cobley, J. Chen, X. Xia, Q. Zhang, M. Yang, E. C. Cho, P. K. Brown, *Acc. Chem. Res.* **2011**, *44*, 914 – 924.
[6] K. D. Gilroy, A. Ruditskiy, H.-C. Peng, D. Qin, Y. Xia, *Chem. Rev.* **2016**, *116*, 10414 – 10472.
[7] H. Zhang, M. Jin, Y. Xia, *Chem. Soc. Rev.* **2012**, *41*, 8035 – 8049.
[8] D. Wang, Y. Li, *Adv. Mater.* **2011**, *23*, 1044 – 1060.
[9] C. J. DeSantis, R. G. Weiner, A. Radmilovic, M. M. Bower, S. E. Skrabalak, *J. Phys. Chem. Lett.* **2013**, *4*, 3072 – 3082.
[10] Z. Peng, H. Yang, *Nano Today* **2009**, *4*, 143 – 164.
[11] Q. Zhang, W. Li, C. Moran, J. Zeng, J. Chen, L.-P. Wen, Y. Xia, *J. Am. Chem. Soc.* **2010**, *132*, 11372 – 11378.
[12] A. M. Michaels, M. Nirmal, L. Brus, *J. Am. Chem. Soc.* **1999**, *121*, 9932 – 9939.
[13] P. Christopher, S. Linic, *J. Am. Chem. Soc.* **2008**, *130*, 11264 – 11265.
[14] B. Hammer, J. Norskov, *Nature* **1995**, *376*, 238 – 240.
[15] M. Haruta, *Catal. Today* **1997**, *36*, 153 – 166.
[16] S. Overbury, V. Schwartz, D. R. Mullins, W. Yan, S. Dai, *J. Catal.* **2006**, *241*, 56 – 65.
[17] T. V. Janssens, A. Carlsson, A. Puig-Molina, B. S. Clausen, *J. Catal.* **2006**, *240*, 108 – 113.
[18] X. Xia, Y. Wang, A. Ruditskiy, Y. Xia, *Adv. Mater.* **2013**, *25*, 6313 – 6333.
[19] Y. Yang, J. Liu, Z.-W. Fu, D. Qin, *J. Am. Chem. Soc.* **2014**, *136*, 8153 – 8156.
[20] J. Lee, J. C. Park, H. Song, *Adv. Mater.* **2008**, *20*, 1523 – 1528.
[21] K. Yu, Z. Wu, Q. Zhao, B. Li, Y. Xie, *J. Phys. Chem. C* **2008**, *112*, 2244 – 2247.
[22] P. M. Arnal, M. Comotti, F. Schüth, *Angew. Chem. Int. Ed.* **2006**, *45*, 8224 – 8227; *Angew. Chem.* **2006**, *118*, 8404 – 8407.
[23] Y. Dai, B. Lim, Y. Yang, C. M. Cobley, W. Li, E. C. Cho, B. Grayson, P. T. Fanson, C. T. Campbell, Y. Sun, *Angew. Chem. Int. Ed.* **2010**, *49*, 8165 – 8168; *Angew. Chem.* **2010**, *122*, 8341 – 8344.
[24] J. Ge, Q. Zhang, T. Zhang, Y. Yin, *Angew. Chem. Int. Ed.* **2008**, *47*, 8924 – 8928; *Angew. Chem.* **2008**, *120*, 9056 – 9060.
[25] P. Lu, C. T. Campbell, Y. Xia, *Nano Lett.* **2013**, *13*, 4957 – 4962.
[26] W. Stöber, A. Fink, E. Bohn, *J. Colloid Interface Sci.* **1968**, *26*, 62 – 69.
[27] Q. Zhang, T. Zhang, J. Ge, Y. Yin, *Nano Lett.* **2008**, *8*, 2867 – 2871.
[28] L. Au, X. Lu, Y. Xia, *Adv. Mater.* **2008**, *20*, 2517 – 2522.
[29] Q. Zhang, W. Li, L. P. Wen, J. Chen, Y. Xia, *Chem. Eur. J.* **2010**, *16*, 10234 – 10239.
[30] L. M. Liz-Marzán, M. Giersig, P. Mulvaney, *Langmuir* **1996**, *12*, 4329 – 4335.
[31] X. Sun, J. Kim, K. D. Gilroy, J. Liu, T. A. F. König, D. Qin, *ACS Nano* **2016**, *10*, 8019 – 8025.
[32] J. F. Moulder, W. F. Stickle, P. E. Sobol, K. D. Bomben, *Handbook of X-ray Photoelectron Spectroscopy, PerkinElmer Corporation, Physical Electronics Division*, **1992**.
[33] K. K. Haldar, S. Kundu, A. Patra, *ACS Appl. Mater. Interfaces* **2014**, *6*, 21946 – 21953.
[34] F. Zhou, Z.-Y. Li, Y. Liu, Y. Xia, *J. Phys. Chem. C* **2008**, *112*, 20233 – 20240.
[35] G. C. Schatz, *Acc. Chem. Res.* **1984**, *17*, 370 – 376.
[36] J. P. Camden, J. A. Dieringer, Y. Wang, D. J. Masiello, L. D. Marks, G. C. Schatz, R. P. Van Duyne, *J. Am. Chem. Soc.* **2008**, *130*, 12616 – 12617.
[37] P. G. Etchegoin, E. Le Ru, *Phys. Chem. Chem. Phys.* **2008**, *10*, 6079 – 6089.
[38] S. M. Ansar, F. S. Ameer, W. Hu, S. Zou, C. U. Pittman, Jr., D. Zhang, *Nano Lett.* **2013**, *13*, 1226 – 1229.
[39] J. Zhang, S. A. Winget, Y. Wu, D. Su, X. Sun, Z.-X. Xie, D. Qin, *ACS Nano* **2016**, *10*, 2607 – 2616.
[40] J. Li, J. Liu, Y. Yang, D. Qin, *J. Am. Chem. Soc.* **2015**, *137*, 7039 – 7042.
[41] J. Li, Y. Wu, X. Sun, J. Liu, S. A. Winget, D. Qin, *ChemNanoMat* **2016**, *2*, 786 – 790.
[42] Y.-F. Huang, H.-P. Zhu, G.-K. Liu, D.-Y. Wu, B. Ren, Z.-Q. Tian, *J. Am. Chem. Soc.* **2010**, *132*, 9244 – 9246.
[43] Y.-F. Huang, D.-Y. Wu, H.-P. Zhu, L.-B. Zhao, G.-K. Liu, B. Ren, Z.-Q. Tian, *Phys. Chem. Chem. Phys.* **2012**, *14*, 8485 – 8497.

Manuscript received: December 20, 2016
Revised: January 22, 2017
Accepted Article published: February 6, 2017
Final Article published: February 22, 2017